

1  
2  
3  
4 **Insolation and Greenhouse Gases Drove Holocene Winter and Spring**  
5 **Warming in Arctic Alaska**

6  
7  
8 William M. Longo<sup>a,b,1,\*</sup>, Yongsong Huang<sup>a,b</sup>, James M. Russell<sup>a,b</sup>, Carrie Morrill<sup>c,d</sup>,  
9 William C. Daniels<sup>a,b</sup>, Anne E. Giblin<sup>e</sup>, Josue Crowther<sup>a</sup>

10  
11 a) Department of Earth, Environmental and Planetary Sciences, Brown University, 324 Brook Street,  
12 Providence, RI 02912

13  
14 b) Institute at Brown for Environment and Society, Brown University, 324 Brook Street, Providence, RI,  
15 02912, USA

16  
17 c) Cooperative Institute for Research in Environmental Sciences, University of Colorado Boulder, 216  
18 UCB, Boulder, CO 80309

19  
20 d) NOAA's National Centers for Environmental Information, Center for Weather and Climate, 325  
21 Broadway, Boulder, CO 80309

22  
23 e) The Ecosystems Center, Marine Biological Laboratory, 7 MBL Street, Woods Hole, MA 02543

24  
25  
26  
27 1) *Current Affiliation*: Department of Marine Chemistry and Geochemistry, 266 Woods Hole Road, Woods  
28 Oceanographic Institution, Woods Hole, MA 02543, USA

29  
30 \* Corresponding Author:

31  
32 William M. Longo  
33 email: [wlongo@whoi.edu](mailto:wlongo@whoi.edu)  
34 Tel: +1 508 289 2921

35  
36  
37  
38 Keywords: Continental biomarkers; Alkenone; Paleoclimatology; Paleolimnology;  
39 Temperature reconstruction; Proxy data-model comparison; Holocene; North America;  
40 Seasonality; Beringia

41 **Abstract**

42

43 Global surface temperature changes and their drivers during the Holocene Epoch remain  
44 controversial. Syntheses of proxy data indicate that global mean annual temperature  
45 declined from the mid-Holocene until the Pre-industrial Era, a trend linked to decreasing  
46 Northern Hemisphere summer insolation. In contrast, global climate models simulate  
47 increasing mean annual temperatures driven by retreating ice sheets and increasing  
48 greenhouse gas concentrations. This proxy-model disagreement may originate from a  
49 warm season bias in Northern Hemisphere proxy reconstructions, highlighting the need  
50 for new proxies that quantify cold season temperature, especially in Arctic regions that  
51 were devoid of continental ice sheets during Holocene. Here, we present a new 16,000-  
52 year winter-spring temperature reconstruction derived from the unsaturation ratio of  
53 alkenones (U) in a continuous sedimentary sequence from Lake E5, northern Alaska. We  
54 employ a thermodynamic lake model to convert alkenone-inferred lake temperatures into  
55 winter-spring air temperature anomalies and we contextualize our proxy reconstruction  
56 with climate model output from the region. Our reconstruction shows that winter-spring  
57 temperatures warmed rapidly during the deglaciation at 16 and 14 thousand years before  
58 present and continued to warm gradually throughout the middle and late Holocene (0.12 -  
59 0.28 °C/thousand years) in concert with regional sea surface temperature and sea ice  
60 records. Our results are consistent with climate model simulations and we attribute  
61 Holocene warming to rising winter-spring insolation, radiative forcing from rising  
62 greenhouse gas concentrations and regional feedbacks. Our reconstructed cold season  
63 warming equaled or exceeded summer cooling according to a regional synthesis of  
64 terrestrial temperature records, suggesting that seasonal biases in temperature  
65 reconstructions may account proxy-model disagreements in Holocene temperature trends  
66 from Eastern Beringia.

67 **1. Introduction**

68

69 Global climate models (GCM) simulate increasing mean annual surface temperature  
70 during the Holocene, primarily driven by retreating Northern Hemisphere ice sheets in  
71 the early Holocene and increasing greenhouse gas (GHG) concentrations after eight  
72 thousand years before present (ka cal BP; Liu et al., 2014). In contrast, syntheses of  
73 globally distributed continental and marine proxy reconstructions indicate that the mean  
74 surface temperature was warm during the early Holocene Climate Optimum (10 – 6 ka  
75 cal BP) and subsequently cooled through the Pre-industrial Era (PI; Marcott et al., 2013).  
76 This cooling is inferred to result from the large ( $\sim 40 \text{ W m}^{-2}$ ) reduction in Northern  
77 Hemisphere summer insolation (NHSI), due to changes in Earth's orbital geometry.  
78 However, orbital forcing caused increases in southern hemisphere summer insolation  
79 over the same interval and no appreciable change in globally and annually averaged  
80 incoming solar radiation (Laskar et al., 2004). Thus, reconstructed early Holocene  
81 warmth and subsequent cooling could only have been realized through strong global  
82 climate feedbacks to NHSI (Marcott et al., 2013), such as reduced albedo from expanded  
83 boreal forests (Foley et al., 1994). Other studies have proposed that a bias in climate  
84 proxies towards boreal summer accounts for the Holocene cooling trend and data-model  
85 mismatch (Liu et al., 2014; Meyer et al., 2015; Baker et al., 2017; Marsicek et al., 2018).  
86 For example, the removal of summer-sensitive marine records from North Atlantic  
87 margins reduced the data-model difference in the global synthesis, but even after  
88 correction the proxy data do not indicate a warming trend (Marsicek et al., 2018), leaving  
89 this “Holocene temperature conundrum” unresolved.

90  
91      Newer paleoclimate records and syntheses have indicated Holocene winter warming,  
92      suggesting that better representation of seasonality in paleoclimate reconstructions could  
93      partly resolve the proxy data-model disagreement (Meyer et al., 2015; Baker et al., 2017;  
94      Marsicek et al., 2018). However, these reconstructions are either limited in duration or  
95      predominantly from terrestrial northern mid-latitude regions that are highly sensitive to  
96      ice sheet forcing (Clark et al., 1999), making them hard to extrapolate to the global mean.  
97      The waning Laurentide Ice Sheet (LIS) was far east of Alaska by the start of the  
98      Holocene Epoch (Dyke, 2004) and had a little impact on Holocene temperatures there  
99      according to proxy data (Kaufman et al., 2004). Therefore, Alaska is a crucial region for  
100     reconstructing seasonally resolved Holocene temperature change in the absence of  
101     significant regional ice sheet feedbacks. New cold season temperature reconstructions  
102     from such regions are essential for identifying seasonal biases in global proxy data and  
103     deconvolving the relative importance of Holocene climate forcing mechanisms and  
104     feedbacks.  
105  
106     Despite the importance of Alaskan cold season climate to resolving Holocene  
107     temperature trends and forcings, there are few continental temperature records  
108     representing the non-summer seasons from the region (Sundqvist et al., 2014). Pollen  
109     assemblages have been used to develop winter temperature reconstructions from lake  
110     sediments (Viau et al. 2008; Bartlein et al. 2011), however tundra plant species with large  
111     geographic ranges result in “non-analog” assemblages preventing accurate winter  
112     temperature estimates (Birks et al., 2011). Oxygen isotope analyses of ice wedges have

113 emerged as techniques to provide winter temperature reconstructions (Opel et al., 2018),  
114 however these archives have rarely provided continuous whole-Holocene records in the  
115 Arctic and are less common or accessible than other continental climate archives. Other  
116 moisture-sensitive oxygen isotope records have been used as winter climate indicators  
117 through their sensitivity to the strength and position of the Aleutian Low (e.g. Anderson  
118 et al., 2005; Clegg et al., 2010). However, interpretations of these records remain  
119 complex (Kaufman et al., 2016) and none of these records directly record temperature  
120 changes.

121

122 In this study, we generate a new winter-spring temperature reconstruction from Arctic  
123 Alaska using sediment cores from Lake E5 (68.642 °N, 149.458 °W, 798 m a.s.l.). To  
124 reconstruct winter-spring temperatures, we utilize alkenones – a series of biomarkers  
125 produced by various species of haptophyte algae (Volkman et al., 1980; Marlowe et al.,  
126 1984; D’Andrea et al., 2006) occurring globally in oceans (Conte et al., 2006) and in  
127 many freshwater lakes (Longo et al., 2018). Our recent work demonstrates that Lake E5  
128 alkenones are produced by the freshwater-dwelling clade of alkenone-producing  
129 Isochrysidales haptophytes (Richter et al., 2019), during the spring transitional season  
130 (Longo et al., 2016; 2018; Richter et al., 2019). The degree of unsaturation of 37-carbon  
131 alkenones records spring lake temperature with high precision ( $\pm 1.37$  °C) by way of the  
132 U index (Brassell et al., 1986) and our site-specific U temperature calibration (Longo et  
133 al., 2016). Lake temperature and lake ice phenology in the spring are controlled by winter  
134 and spring air temperatures due to the high thermal inertia of lakes and their accumulated  
135 winter ice cover (Palecki and Barry, 1986; Assel and Robertson, 1995; Livingstone,

136 1997; Magnuson et al., 2000; Arp et al., 2013). Accordingly, the alkenone proxy  
137 responds strongly to winter lake ice conditions and correlates with air temperatures of the  
138 late winter and spring in many freshwater lakes (Longo et al., 2018).

139

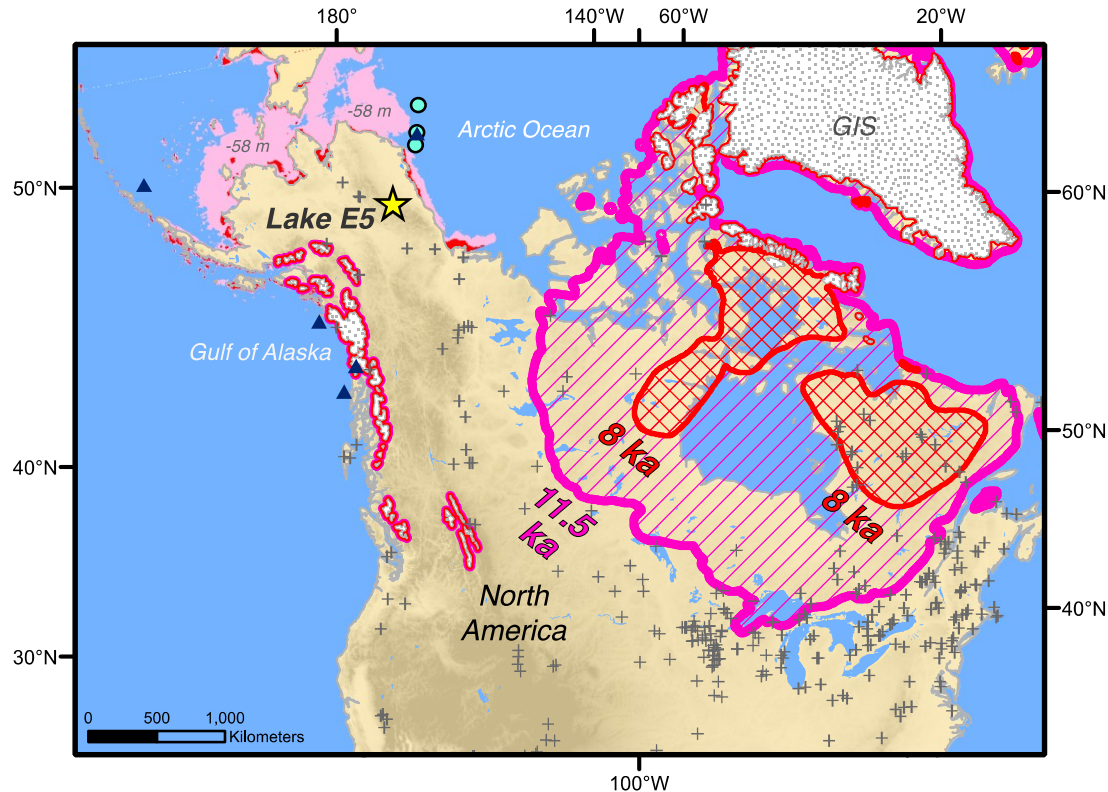
140 We carried out a series of modeling experiments by forcing a one-dimensional  
141 thermodynamic lake model (Hostetler and Bartlein, 1990) calibrated to our study site,  
142 with a series of Holocene climate simulations from the Proxy Model Intercomparison  
143 Project Phase III (PMIP3; Braconnot et al., 2012). Results from these experiments  
144 support the interpretation that alkenones record winter-spring air temperature changes  
145 and they quantify the lake temperature-air temperature relationship at Lake E5. We  
146 combine our novel winter-spring temperature reconstruction with PMIP3 and transient  
147 climate model output from the region to elucidate Holocene winter-spring temperature  
148 evolution in Arctic Alaska and identify forcing mechanisms driving Holocene  
149 temperature trends.

150    **2. Regional Setting**

151

152    The North Slope of Alaska lies between 68°N and 71°N and comprises three  
153    physiographic regions—the Brooks Range Mountains, Arctic Foothills and Arctic  
154    Coastal Plain—that are situated south to north along a gradient of decreasing temperature  
155    and elevation (Hobbie and Huryn, 2012). Lake E5 is a kettle lake (Surface Area = 0.109  
156    km<sup>2</sup>; Maximum Depth = 12.7 m; Mean Depth = 6.33 m) situated in the Arctic foothills on  
157    an upland tundra landscape underlain by continuous permafrost (Fig. 1). The catchment  
158    was free of glaciers throughout the last glacial period (Hamilton, 1982) and the lake  
159    underwent continuous sedimentation dating to 32 ka cal BP offering a rare uninterrupted  
160    record of the Last Glacial Maximum (LGM), deglaciation, and Holocene (Eisner and  
161    Colinvaux, 1992; Vachula et al., 2019). Lake E5 is oligotrophic and ice-free from mid-  
162    June through late September. Mean annual air temperatures at Lake E5 are -8 °C with  
163    low winter temperatures of -35 °C and high summer temperatures of 20 °C (Hobbie and  
164    Huryn, 2013). Mean annual precipitation for the region is 292 mm yr<sup>-1</sup> and mean annual  
165    evapotranspiration is 127 mm yr<sup>-1</sup> (Dery et al., 2005).

166



167

168 **Fig. 1. Study site and early Holocene ice sheet extent.** Map of North America showing the extent of the  
 169 LIS at 11.5 ka cal BP (magenta hatch) and 8 ka cal BP (red cross-hatch; Dyke et al., 2004), and estimated  
 170 extent of exposed shelf surrounding Alaska at 11.5 ka cal BP (pink shading) and 8 ka cal BP (red shading;  
 171 Manley et al., 2002), respectively. Lake E5 is marked with the yellow star. "GIS" refers to the Greenland Ice  
 172 Sheet. Records used in the recent pollen synthesis ("+" symbols; Marsicek et al., 2018) are dominated by  
 173 mid-latitude sites. Sea surface temperature (navy triangles) and sea-ice (teal circles) reconstructions  
 174 discussed in the text are indicated.

175

176 **3. Materials and Methods**

177 *3.1. Sediment Core Retrieval, Processing and Chronology*

178

179 Sediment cores were collected from the deepest part of Lakes E5 in May, 2014 over ~1 m  
180 of lake ice cover, using a piston corer for surface cores and a modified Livingstone corer  
181 for subsequent cores. Six vertical meters of sediment were collected, the top 4.8 m of  
182 which resulted in a continuous sedimentary record. Cores were returned to Brown  
183 University, logged visually, and were imaged and logged for Magnetic Susceptibility and  
184 X-ray Fluorescence using a Geo-Tek™ multi-sensor core logger. Overlapping cores were  
185 aligned based on visually distinct beds and lithological parameters including organic  
186 carbon content, magnetic susceptibility, and elemental data. Aligned cores were spliced  
187 to create a continuous 4.8 m sedimentary sequence.

188

189 1-2 cm thick samples were aliquoted and frozen for radiocarbon dating from the working  
190 halves of split and logged cores. For radiocarbon processing, ~ 5 cm<sup>3</sup> subsamples were  
191 sieved at 500 and 150 µm. From the sieved fractions, terrestrial plant and insect  
192 macrofossils were collected under a dissecting microscope, characterized, and treated for  
193 ultra-microscale radiocarbon analysis (Shah Walter et al., 2015). The full radiocarbon and  
194 <sup>210</sup>Pb chronology is published by Vachula et al. (2019; Fig. S1) and consists of 16  
195 radiocarbon dates and <sup>210</sup>Pb dating in the uppermost sediments. Holocene aged sediments  
196 consist of brown thickly bedded silts, deglacial sediments consist of black and green  
197 laminated silts and clayey silts.

198

199 3.2. Alkenone Analysis and U Temperature Determinations

200

201 Alkenone analysis was carried out using established methods (Longo et al., 2016).  
202 Sediment cores were sampled in 1 cm sections and samples were freeze-dried,  
203 homogenized and extracted using an accelerated solvent extraction system (ASE200;  
204 Dionex). Neutral lipids were separated from fatty acids by flash column chromatography  
205 using Supelco™ Supelclean LC-NH2 powder. A ketone fraction was eluted from the  
206 neutral lipids with dichloromethane by way of flash column chromatography with silica  
207 gel. Ketone fractions were saponified before analysis by GC-MS to check peak purity and  
208 further analyzed by GC-FID for quantification.

209

210 GC-MS analysis was performed using an Agilent 6890N GC system coupled to an  
211 Agilent 5973N quadrupole mass spectrometer and GC-FID analysis was performed  
212 using an Agilent 7890B GC system with the operating conditions outlined by Longo et al.  
213 (2016). All GC-MS and GC-FID analyses were performed with a VF-200ms 60m  
214 capillary column, allowing for full separation of Group I alkenone distributions (Longo et  
215 al., 2013). Alkenone quantification was accomplished using 18-pentatriacontane as an  
216 internal standard and all injections were made within a narrow dynamic range of ~2-20  
217 ng of C<sub>37</sub> alkenones on column to reduce analytical uncertainties in alkenone  
218 quantification. Analytical error on U-inferred temperatures is  $\pm 0.20$  °C (1SD) based on  
219 replicate analyses of alkenone standards and sediment core samples. The uncertainty in  
220 the temperature calibration ( $\pm 1.37$  °C) includes this analytical error (Longo et al., 2016).

221

222 3.3. *Proxy Fundamentals and Interpretation*

223

224 Alkenones in Lake E5 and nearby Toolik Lake (68.632 °N, 149.602 °W) are produced by  
225 the Group I phylotype of Isochrysidales haptophyte algae, which is the dominant group in  
226 freshwater environments (Longo et al., 2016; 2018; Richter et al., 2019). The relationship  
227 between Group I alkenone unsaturation and temperature is broadly consistent across sites  
228 in the Northern Hemisphere (D'Andrea et al., 2011; 2016; Longo et al., 2016; 2018) and  
229 has been robustly quantified at Toolik Lake (Longo et al., 2016). An in situ calibration  
230 from Lake E5 indicates that Lake E5 and Toolik Lake calibrations are statistically  
231 indistinguishable (Fig. S2). Therefore, the published Toolik Lake calibration (Longo et  
232 al., 2016) is used for lake water temperature determinations.

233

234 Group I Isochrysidales haptophytes are most abundant in the water column of Lake E5  
235 and its neighboring lakes in the spring, during the periods of partial ice cover, isothermal  
236 spring mixing, and at the onset of thermal stratification (Richter et al., 2019). We  
237 collectively refer to these periods, which occur during the month of June at Lake E5, as  
238 the spring transitional season. Geochemical and observational data have shown that  
239 alkenone production and deposition occur during this spring transitional season, which is  
240 characterized by lake surface temperatures ranging from 2 to 15 °C (Longo et al., 2016;  
241 2018). These springtime sedimentary fluxes of Group I alkenones are also seen in  
242 Norway (D'Andrea et al., 2016), whereas southwest Greenland lakes show a slightly later  
243 peak flux, shortly after ice out (D'Andrea et al., 2011).

244

245 Spring lake temperatures and lake ice break-up are dominantly influenced by the mean  
246 temperature of the preceding 1-6 months, through the effects of winter and early spring  
247 temperature on lake ice accumulation and the timing of spring thaw (Palecki and Barry,  
248 1986; Robertson et al., 1992; Assel and Roberston, 1995; Livingstone, 1997; Magnuson  
249 et al., 2000; Arp et al., 2013). Accordingly, alkenone unsaturation has been shown to  
250 correlate with late winter and spring air temperature (Longo et al., 2018). Additionally,  
251 surface sediment and sediment trap data from Toolik Lake with accompanying year-  
252 round lake ice phenology data, corroborate the interpretation of the proxy as reflecting  
253 winter-spring climate, with colder U-inferred lake temperatures corresponding with  
254 longer ice-out periods and later ice-off dates (Fig. S3; Toolik Environmental Data Center  
255 Team, 2016). Within our proxy framework, these data suggest that colder temperatures in  
256 the winter and spring, which result in more ice accumulation on the lake surface, have  
257 lasting effects on spring lake temperature through the thermodynamic requirement of  
258 melting a thicker ice cover and the delaying of summer lake surface warming through  
259 extended ice cover. The Group I haptophytes have a consistent spring bloom timing and  
260 therefore record spring lake temperatures dominated by these seasonal lake ice dynamics.

261  
262 Changes in alkenone-producing haptophyte species have been known to overprint  
263 alkenone-inferred temperatures in lakes (Randlett et al., 2014). The RIK<sub>37</sub> index (Longo  
264 et al., 2016) was calculated for all samples to evaluate species effects, which were absent  
265 from the record (Fig. S4).

266

267

268 3.4. *Lake Model Description, Parameterization and Validation*

269

270 The Hostetler and Bartlein lake model is a one-dimensional energy- and water-balance  
271 model that requires inputs for near-surface air temperature, humidity, wind speed, surface  
272 incident shortwave and longwave radiation, surface pressure, precipitation, and runoff  
273 (Hostetler and Bartlein, 1990, Dee et al., 2018). Meteorological inputs from 1994 – 2015  
274 CE were obtained from the Toolik Environmental Data Center (5 m air temperature, 5 m  
275 relative humidity, 5 m wind speed, surface incident shortwave radiation, surface air  
276 pressure; Toolik Environmental Data Center Team, 2016) and from the Imnaviat Creek  
277 Snotel site (precipitation; SNOTEL, site 968). Toolik Lake is approximately 5 km west of  
278 Lake E5 and the Imnaviat Creek site is approximately 7 km east of Lake E5. Downward  
279 longwave radiation values are available only for the end of the record (May 2013-  
280 December 2014). To extend longwave values back to 1994, a multiple linear regression  
281 relationship between this variable, air temperature, and relative humidity was calculated  
282 for the 19-month period when all three variables were measured. Toolik EDC  
283 meteorological data are hourly and the Snotel data are daily. For missing values in the  
284 meterological dataset, data gaps less than or equal to six hours in duration were filled  
285 using linear interpolation. Daily precipitation amounts were divided evenly across the 24-  
286 hour period and missing values for precipitation were set to zero.

287

288 A series of present-day simulations were used to determine the most appropriate values  
289 for several adjustable lake-specific parameters in the lake model. To carry out these  
290 simulations, the model was run with a 10-year spin-up period using repeated 2008 data,

291 followed by the 21-year meteorological dataset. The lake-specific parameters include the  
292 neutral drag coefficient, the albedos of snow and melting snow, and the shortwave  
293 extinction coefficient. These parameters were calibrated by comparing lake model output  
294 from 2008-2014 CE to limnological data obtained from both the Toolik Environmental  
295 Data Center (Toolik Environmental Data Center Team, 2016) and the Arctic Long Term  
296 Ecological Research program (ARC LTER database; NSF-DEB-1637459), including  
297 mean lake temperature, maximum summer lake temperature, break-up date, freeze-up  
298 date, and mixing depth. The 2008-2014 CE period was selected for validation because of  
299 its comprehensive data coverage in both meteorological data and limnological data.  
300 Sensitivity tests indicated that the neutral drag coefficient and albedo terms had the  
301 greatest effects on modeled lake temperatures. The neutral drag coefficient was set to  
302 0.002 and the albedos of slush and snow were set to 0.4 and 0.7, respectively. Lake size  
303 had only minimal effects (< 0.3 °C difference in average spring lake temperature between  
304 Lake E5 and Toolik Lake-sized basins). The fully calibrated lake model was then  
305 employed for Lake E5 6 ka experiments.

306  
307 For visualization of model performance, lake model output at 1.5 m depth was compared  
308 with measured lake temperature at 1 – 2.2 m depth, and seasonal ice cover at Toolik Lake  
309 (Fig. S5). Observed lake temperature is derived from a fixed sensor in the lake therefore  
310 its depth varies between 1 and 2.2 m with lake level fluctuations (Toolik Environmental  
311 Data Center Team, 2016).

312  
313

314 *3.5. GCM Output and Mid-Holocene Lake Model Simulations*

315

316 GCM outputs from PMIP3 (Braconnot et al., 2012) and three transient simulations –  
317 CCSM3 (Liu et al., 2009), LOVECLIM (Timm and Timmermann, 2007), and FAMOUS  
318 (Smith and Gregory, 2012; Liu et al., 2014) – were extracted from the four gridcells most  
319 proximal to Toolik Lake and Lake E5. 6 ka vs. Pre-Industrial (PI) anomalies were  
320 calculated from PMIP3 simulations using the 6 ka and PI outputs. 6 ka vs. Present-Day  
321 (PD) anomalies were calculated using the PMIP3 6 ka outputs and modern outputs (1981-  
322 2005 CE) from CMIP5 historical simulations. For the transient simulations, anomalies  
323 were calculated as the average temperature from 7 – 5 ka cal BP minus the average  
324 temperature at 1750 – 1850 CE. The same PI reference period (1750-1850 CE) was  
325 applied to calculate alkenone-derived air temperature anomalies.

326

327 Mid-Holocene (6 ka) lake model simulations were carried out using climatology outputs  
328 from eight GCMs participating in PMIP3 (Braconnot et al., 2012) with the necessary  
329 variables for the lake model (BCC-CSM1-1, CCSM4, CNRM-CM5, GISS-E2-R,  
330 HadGEM2-ES, IPSL-CM5A-LR, MIROC-ESM, MRI-CGCM3). 6 ka input datasets for  
331 the lake model were developed by applying the change in climatology between 6 ka and  
332 PD simulated by each PMIP3 model to the modern meteorological (control) inputs. This  
333 approach alleviates issues with biases in climate model output for present-day climate,  
334 although biases can still impact the magnitude of the modeled change between 6 ka and  
335 PD. To generate climatologies, at least 100 years of GCM output was averaged for the 6  
336 ka time period, and 75 years of GCM output (1981-2005 CE for three ensemble

337 members) was averaged for the PD from the CMIP5 historical simulations. For most of  
338 the meteorological variables, the percentage change between the modern and 6 ka  
339 simulations was used to scale the observational data for input to the lake model. For air  
340 temperature, the only variable that can have negative values, the temperature anomaly  
341 was directly applied to the modern dataset. Likewise, the anomalous wind speed change  
342 for the MIROC-ESM and IPSL-CM5A-LR models was directly applied given their small  
343 (<2 m/s) climatological values for this variable that yield unrealistically large percentage  
344 changes between the 6 ka and PD time periods. Given the dependence of relative  
345 humidity on temperature, this variable was scaled by first converting to specific humidity  
346 and applying the modeled percentage change in specific humidity, then converting back  
347 to relative humidity using the anomalous temperature value.

348

349 Each 6 ka lake model simulation was first spun up for 10 years to reach equilibrium as  
350 defined by stabilization of lake temperature, and then run over the 21-year meteorological  
351 period, ensuring that a full range of inter-annual climate variability was captured in the  
352 simulations.

353

### 354 *3.6. Simulated Spring Lake Temperature vs. Winter-Spring Air Temperature*

355

356 For comparison to the alkenone proxy, the average spring lake temperature was extracted  
357 from model outputs as the averaged epilimnion + metalimnion temperature 30 days  
358 before and after the average ice-off date. These criteria were chosen based on  
359 observations of alkenones in Lake E5 and Toolik Lake (Longo et al., 2016; 2018). The

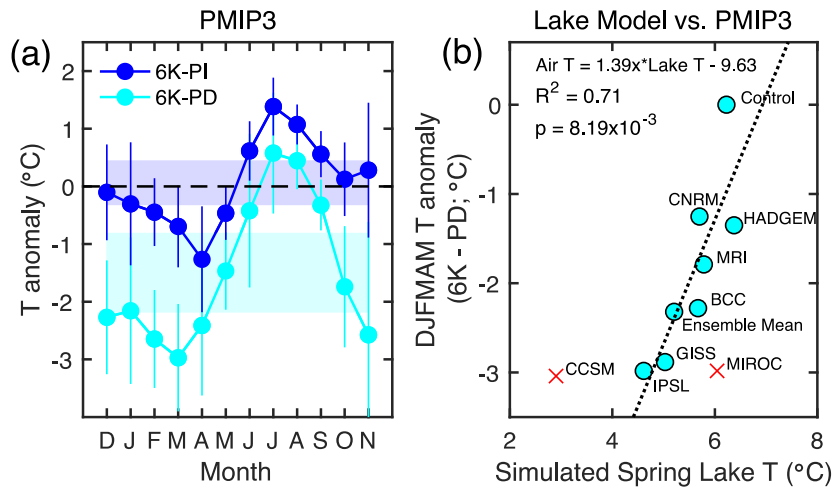
360 regression of this simulated spring lake temperature vs. DJFMAM air temperature from  
361 several 6 ka lake model simulations was used to transform proxy-derived spring lake  
362 temperature estimates into DJFMAM air temperatures (Fig. 2). Each point in the ordinary  
363 least squares regression represents a lake model simulation forced by a single 6 ka  
364 climate model input (abbreviated, respectively, from above: BCC, CCSM, CNRM, GISS,  
365 HADGEM, IPSL, MIROC, MRI), the ensemble mean, or the control run with modern  
366 meteorological data. Outputs produced by CCSM were not included in the regression  
367 because they produced anomalously cold lake temperatures due to anomalously cold June  
368 air temperatures relative to the other ensemble members (-3SD from the ensemble mean).  
369 These cold June temperatures prevented stratification in the early summer and thus  
370 caused a lake stratification regime shift in the lake model, making the resulting spring  
371 lake temperatures incomparable with the other simulations. The MIROC output was also  
372 excluded from the regressions because it produced anomalously warm spring lake  
373 temperatures relative to other simulations and forced the regression to inadequately fit the  
374 control simulation. (Exclusion of MIROC resulted in only minor changes in the  
375 regression slopes; Fig. S6).

376

377 Regressions demonstrate that spring lake temperature and ice-off date are strongly  
378 correlated with winter-spring (DJFMAM) air temperature (Figs. 2, S6). We used the  
379 regression to transform reconstructed spring lake temperatures at Lake E5 into DJFMAM  
380 air temperature estimates, which are displayed as anomalies relative to pre-industrial (PI;  
381 Fig. S7). The transfer function assumes that the regression slope is stationary throughout  
382 the Holocene. We suggest this assumption is reasonable given the relatively small range

383 in spring lake temperature change over this period, however a formal test of this  
384 assumption is not possible with the available climate model output.

385



386

387 **Fig. 2. Simulated mid-Holocene temperatures at Lake E5.** (a) PMIP3 ensemble mean surface air  
388 temperatures at Lake E5 at 6 ka relative to the PI (pre-industrial) and PD (present day), shown as monthly  
389 (points) and mean annual (shaded regions) anomalies. (b) The linear regression of lake model simulated  
390 spring lake temperature at 6 ka with PMIP3 simulated winter-spring air temperature anomalies at 6 ka  
391 relative to the PD. Points are labeled by the PMIP3 output (ensemble mean or individual models) used to  
392 drive lake model simulations. The simulation labeled "control" was forced with the modern meteorological  
393 data. Two outlying simulations are marked with a red "x" and discussed in the text.

394

395

### 396 3.7. Statistical Analyses

397

398 Temperature trends for Holocene time series intervals (11.7 ka cal BP – PI and 8 ka cal  
399 BP – PI) were determined using ordinary least squares regression and their significance  
400 was assessed using an F-test. To incorporate the uncertainties of the U temperature  
401 determinations into our analysis of temperature trends, we carried out Monte Carlo  
402 simulations. The experiments simulate 1,000 realizations of the alkenone time series  
403 drawn at random given the 1SD uncertainty of  $\pm 1.37$  °C. Ordinary least squares

404 regressions were carried out for each of the 1,000 simulations and the SD of the resulting  
405 regression coefficients is used to provide a comprehensive estimate of the uncertainty in  
406 temperature trends. The same Monte Carlo experiments were used to determine the  
407 uncertainty of reported mean temperatures over discrete intervals (e.g. Early Holocene, 8  
408 – 6 ka cal BP cold period, etc.) and spring lake temperature changes ( $\Delta T$ ) associated with  
409 warming events. The statistical significance of rapid warming events was checked using  
410 paired, two-tailed T-tests. All uncertainties are reported as  $\pm 1\text{SD}$  unless noted otherwise.

411 **4. Results and Discussion**

412 *4.1. Rapid Deglacial Warming of Spring Lake Temperatures*

413

414 Alkenones appear in the Lake E5 record at 16.2 ka cal BP and indicate three stages of  
415 rapid deglacial warming (Fig. 3). The first warming, from 16.2 – 15.5 ka cal BP  
416 represents a  $\sim$ 2 °C increase in lake temperature and coincides with regional climate  
417 changes including the second phase of alpine glacial retreat in the Brooks Range  
418 (Pendleton et al., 2015) and warming in Northwestern Alaska (Kurek et al., 2009). The  
419 second warming stage of  $2.2 \pm 0.5$  °C occurred from 14.5 – 13.7 ka cal BP, culminating  
420 in the most rapid and sustained temperature increase in the record. This major warming  
421 event is associated with contemporaneous records of vegetation change, soil development  
422 and thermal degradation of permafrost from the region (Anderson and Brubaker, 1994;  
423 Mann et al., 2002; 2010; Abbott et al., 2010). Temperatures then warmed again from 12.0  
424 – 11.6 ka cal BP by  $\sim$ 1 °C, marking the onset of Holocene climate (Fig. 3).

425

426 Spring lake temperatures at Lake E5 prior to 14.5 ka cal BP averaged  $4.00 \pm 1.49$  °C and  
427 were accompanied by the highest  $C_{37}$  alkenone concentrations in the record (Figs. 3, S4).  
428 These data are consistent with prolonged springtime alkenone production during a cold  
429 polymictic stratification regime. We infer a dimictic stratification regime for spring lake  
430 temperatures above 5 °C based on modern observations that Lake E5 begins to thermally  
431 stratify in the spring when lake temperatures reach 5 – 6 °C (ARC LTER database).  
432 Therefore, the prominent warming event from 14.5 – 13.7 ka cal BP likely caused a shift  
433 in Lake E5’s stratification regime.

434

435 The 14.5 – 13.7 ka cal BP warming in our record corresponds with the Bølling-Allerød  
436 winter warming reconstructed from ice wedge oxygen isotopes at Barrow in coastal  
437 north-central Alaska (Meyer et al., 2010). Ice wedges derive from winter precipitation  
438 and therefore their  $\delta^{18}\text{O}$  signatures reflect winter climate and primarily, winter  
439 temperature (Meyer et al., 2010; Opel et al., 2018). Our record corroborates findings by  
440 Meyer et al. (2010) that the maximal Bølling-Allerød winter warming in the region  
441 lagged warming in Greenland by ~1 ka. However, the records diverge during the  
442 Younger Dryas (YD), as Lake E5 alkenones do not record the severe winter cooling  
443 indicated by the Barrow Ice Wedge System (Meyer et al., 2010). This also contrasts with  
444 records from the North Atlantic where YD cooling is thought to be enhanced during  
445 winter due to strong sea-ice feedbacks (Denton et al., 2005). The YD is only seen  
446 sporadically in terrestrial records from the region (Kokorowski et al., 2008), but is  
447 recorded prominently in north-central Alaskan paleoecological records (Mann et al.,  
448 2002; 2010) and temperature reconstructions (Meyer et al., 2010; Gaglioti et al., 2017).

449

450 Younger Dryas climate impacts are likely spatially complex in northern Alaska due to sea  
451 ice export from the Chukchi and Beaufort Seas driven by Bering Strait resubmergence  
452 and deglacial sea level rise (Bradley et al., 2008). Therefore, one potential explanation for  
453 the lack of correspondence between YD temperatures reconstructed at Lake E5 vs.  
454 records from Barrow and North-central Alaska could be regional heterogeneities in the  
455 feedbacks and mitigating factors that determined the magnitude of YD cooling. We must  
456 also consider the possibility that the YD signal at Lake E5 was damped or modified by

457 aforementioned changes in the stratification regime that occurred around this time.  
458 Despite this lack of regional correspondence in YD cooling, deglacial warming events at  
459 Lake E5 align well with several other temperature, hydrological and paleoecological  
460 reconstructions (e.g. Abbott et al., 2010; Mann et al., 2010; Meyer et al., 2010; Pendleton  
461 et al., 2015) lending support to our reconstructed deglacial lake temperatures.

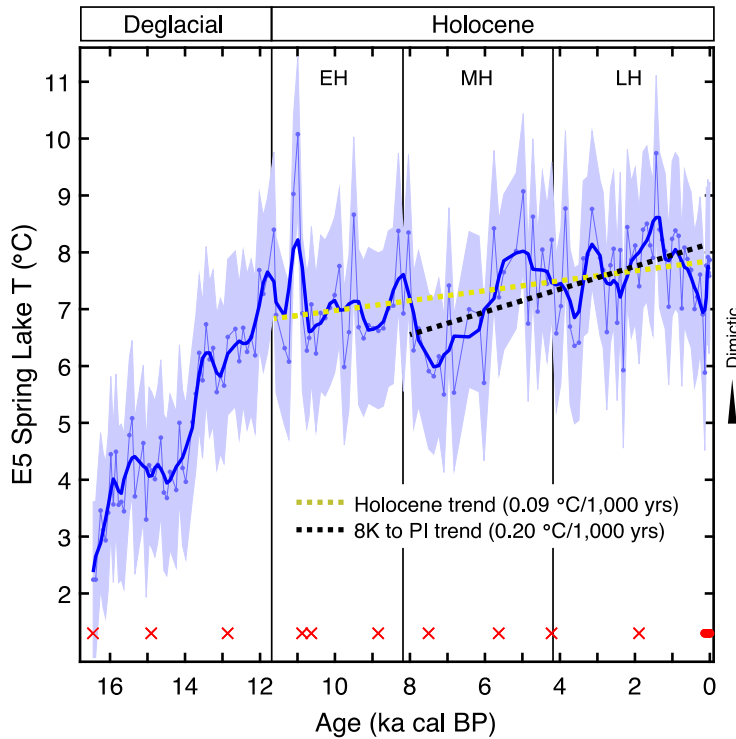
462

463 *4.2. Holocene Winter-Spring Temperature and Comparison with GCMs*

464

465 Gradual warming dominates the Holocene spring lake temperature trend in our record  
466 (11.7 ka cal BP – PI;  $0.087^{\circ}\text{C}/\text{ka}$ ;  $p = 1.12 \times 10^{-3}$ ). The early to mid-Holocene transition  
467 (EMHT) at 8 ka cal BP, marked the collapse of the LIS and Earth's full transition to post-  
468 glacial boundary conditions (Stager and Mayewski, 1997), therefore we also consider the  
469 warming trend that began during this event and persisted throughout the middle and Late  
470 Holocene (8 ka cal BP – PI;  $0.20^{\circ}\text{C}/\text{ka}$ ;  $p = 6.35 \times 10^{-5}$ ). The post-EMHT amplitude of  
471 warming exceeds the Holocene average owing to a local temperature minimum at  $\sim 7$  ka  
472 cal BP driven, in part, by multi-centennial variability. Both trends are robust after  
473 accounting for the uncertainty in U temperature determinations (Fig. 3; Table S3).

474



475

476 **Fig. 3. 16,000-year record of spring lake temperature from Lake E5.** The data is overlaid with a  
 477 smoothing function (LOWESS; span = 7;  $\alpha = 0.05$ ) and the uncertainty in the reconstruction is plotted as the  
 478 light blue error envelope ( $\pm 1\text{SD}$ ). Statistically significant warming trends are shown for the whole Holocene  
 479 (yellow dashed line) and 8 ka cal BP – PI (black dashed line). Age control points are plotted in red along the  
 480 bottom (“X” indicates  $^{14}\text{C}$  and “o” indicates  $^{210}\text{Pb}$ ). EH, MH and LH refer to the early, middle and late  
 481 Holocene, respectively. A dimictic stratification regime is inferred for spring lake temperatures above 5 °C  
 482 based on modern observations.

483

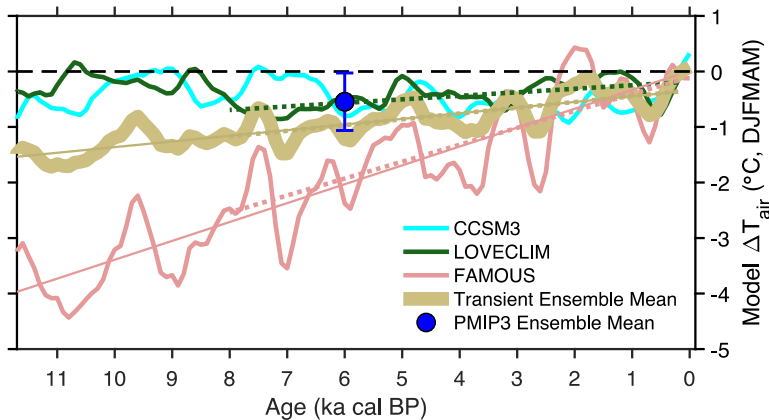
484

485 Spring lake temperatures scale linearly with winter-spring air temperature according to  
 486 our 6 ka lake model simulations, and are suppressed relative to air temperature changes.  
 487 (Fig. 2). We used this relationship to estimate Holocene cold season air temperature and  
 488 find that the warming trends are 0.12 °C/ka (11.7 ka cal BP – PI) and 0.28 °C/ka (8 ka cal  
 489 BP – PI). Thus, we estimate that cold season air temperatures warmed by 1.4 °C over the  
 490 whole Holocene and warmed by 2.2 °C after the EMHT. Although the post-EMHT  
 491 warming trend may be enhanced by stochastic, high-frequency variability, the pattern of

492 change is conserved after smoothing the record (Fig. S7), suggesting the acceleration of  
493 warming in the mid- to late Holocene is a robust feature of the reconstruction.

494

495 The magnitudes and rates of reconstructed winter-spring temperature change at Lake E5  
496 are in general agreement with GCM simulations. An ensemble of GCM output from the  
497 Proxy Model Intercomparison Project Phase III (PMIP3; Braconnot et al., 2012)  
498 simulates 0.5 °C cooler winter and spring temperatures at 6 ka relative to the PI at Lake  
499 E5 (Fig. 4), in accordance with the reconstructed temperature minimum at 8 – 6 ka cal BP  
500 (Fig. 3). Furthermore, the transient simulation by the Loch-Vecode-Ecbilt-Clio-Agism  
501 Model (LOVECLIM, Timm and Timmermann, 2007) simulates moderately warm early  
502 Holocene temperatures at Lake E5 followed by a temperature minimum at 7.1 ka cal BP  
503 and subsequent warming (Fig. 4). The transient simulation from Community Climate  
504 System Model 3 (CCSM3; Liu et al., 2009) reproduces the mild early Holocene  
505 temperatures seen in LOVECLIM and the proxy data, however it also simulates a subtle  
506 mid- to late Holocene cooling trend (Fig. 4). A transient simulation from the Fast Met.  
507 Office and UK universities Simulator (FAMOUS; Smith and Gregory, 2012) indicates  
508 pronounced Holocene warming occurring over both intervals in question (11.7 ka cal BP  
509 – PI and 8 ka cal BP – PI; Fig. 4). LOVECLIM, the transient ensemble mean (including  
510 LOVECLIM, CCSM3 and FAMOUS) and FAMOUS simulate warming trends of 0.064,  
511 0.10 and 0.31 °C/ka, respectively, from 8 ka cal BP to the PI (Fig. 4; Table 1). Our  
512 reconstructed warming of 0.28 °C/ka falls within this range of GCM estimates.  
513 Furthermore, the whole Holocene trend derived from proxy data (0.12 °C/ka) is similar to  
514 the transient ensemble mean (0.10 °C/ka) for the same interval (Figure 4; Table 1).



517 **Fig. 4. PMIP3 and Transient simulations of winter-spring air temperature anomalies (vs. PI) at Lake**  
 518 **E5.** The PMIP3 Ensemble Mean is the average of the 8 simulations used in lake model experiments. The  
 519 Transient Ensemble Mean is the average of CCSM3, LOVECLIM, and FAMOUS simulations. All transient  
 520 simulations were resampled and smoothed for comparison with the Lake E5 reconstruction. All significant ( $p$   
 521  $< 0.01$ ) post-EMHT warming trends are shown with dashed lines. Significant ( $p < 0.01$ ) warming trends over  
 522 the entire Holocene are shown with solid lines.

**Table 1.** Summary of Holocene winter-spring temperature trends in proxy data and models.

Time Series	11.7 ka – PI	8 ka – PI
Alkenone-inferred (Spring Lake T, °C/ka)	0.087	0.20
Alkenone-inferred (DJFMAM Air T, °C/ka)	0.12	0.28
LOVECLIM (DJFMAM Air T, °C/ka)	NT	0.064
CCSM3 (DJFMAM Air T, °C/ka)	-0.025	-0.049
FAMOUS (DJFMAM Air T, °C/ka)	0.34	0.31
Transient Ensemble Mean (DJFMAM Air T, °C/ka)	0.10	0.11

NT = no significant trend

All indicated numeric trends are significant ( $p < 0.01$ )

Positive (negative) trends indicate Holocene warming (cooling)

531 4.3. *Insolation and Greenhouse Gas Forcing of Holocene Winter-Spring Temperature*

532

533 The distinct structure of Holocene warming recorded at Lake E5 diverges from other cold  
534 season temperature reconstructions in Eurasia and North America (Meyer et al., 2015;  
535 Baker et al., 2017; Marsicek et al., 2018), and may therefore offer new insight into Arctic  
536 cold season climate forcing mechanisms (Fig. 5). The temperature minimum from 8 – 6  
537 ka cal BP at Lake E5 is not observed in these other cold season records (Baker et al.,  
538 2017; Marsicek et al., 2018). Notably, it occurs during Holocene minima in winter-spring  
539 (DJFMAM) insolation and GHG radiative forcing. These forcings increase by  
540 approximately  $3.5 \text{ W m}^{-2}$  and  $0.5 \text{ W m}^{-2}$ , respectively, from 8 ka cal BP to the PI and are  
541 accompanied by progressive cold season warming at Lake E5. Insolation during the  
542 opposite half year (JJASON) provides a much stronger and opposite forcing ( $-15 \text{ W m}^{-2}$ ),  
543 which is doubled when considering summer insolation alone (JJA;  $-36 \text{ W m}^{-2}$ ). Despite  
544 its larger amplitude, NHSI did not trigger Holocene cold season cooling according to our  
545 reconstruction and GCM simulations.

546

547 In addition to orbital and GHG forcing, ice sheet retreat has been identified as a major  
548 driver of winter warming during the Holocene in North America, Eurasia, and the North  
549 Atlantic (Liu et al., 2014; Baker et al., 2017; Marsicek et al., 2018). Our new  
550 reconstruction deviates from these records in the early Holocene, revealing a spatially  
551 variable imprint of ice sheet forcing on Holocene cold season climate. At Lake E5, the  
552 slightly warmer winter-spring temperatures in the early Holocene (as compared with 8 –  
553 6 ka cal BP) are consistent with a reduced LIS that had retreated into present day north-

554 central and northeastern Canada, more than 1,000 km east of Lake E5 (Fig. 1, Dyke et al.,  
555 2004). We observe periods of warmth and even a slight cooling as retreat continued  
556 during the early Holocene, indicating that ice sheet effects were minimal or non-existent  
557 at our site (Fig. 5). In contrast, a recent synthesis of pollen records from North America  
558 and Europe shows cold season warming from the early to mid-Holocene (Fig. 5;  
559 Marsicek et al., 2018), as does a speleothem-based winter temperature reconstruction  
560 from Eurasia (Baker et al., 2017). These reconstructions are dominated by sites proximal  
561 to the continental ice sheets, within the influence of northerly winds induced by  
562 anticyclonic circulation over the ice sheet (Clark et al., 1999), or in the path of  
563 downstream atmospheric flow (Baker et al., 2017). We conclude that the pattern of  
564 temperature change in Arctic Alaska, including mild winter-spring temperatures in the  
565 early Holocene and pronounced warming after the EMHT, was primarily forced by  
566 winter-spring insolation and GHG forcing with minimal influences from ice sheet retreat  
567 despite its prominent role at other northern mid-latitude sites.

568

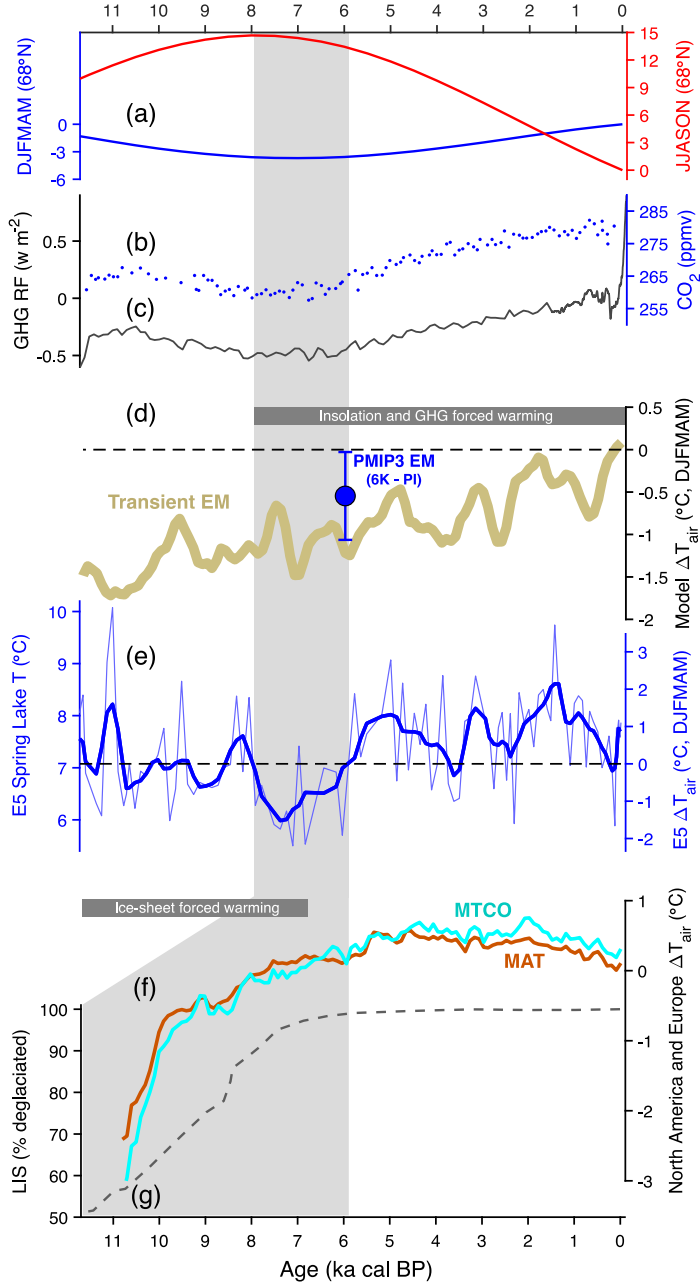


**Fig. 5. Holocene cold season temperature in the context of climate forcings.** (a) Mean insolation ( $\text{W m}^{-2}$ ,  $68^{\circ}\text{N}$ ) for the half year corresponding to the alkenone proxy (DJFMAM) and the opposing half year (JJASON). (b)  $\text{CO}_2$  concentrations recorded in Antarctic Ice (Monnin et al., 2001). (c) GHG radiative forcing from  $\text{CO}_2$ ,  $\text{CH}_4$ , and  $\text{NO}_2$  relative to the PI (Joos and Spahni, 2007). (d) GCM simulated cold season temperature anomalies (vs. PI) at Lake E5 from the 6 ka PMIP3 ensemble mean (blue dot), and the transient ensemble mean (gold). (e) Alkenone-inferred spring lake temperature (left axis) used to estimate DJFMAM air temperature anomalies (vs. PI) at Lake E5 (right axis). (f) Pollen proxy synthesis of mean annual temperature (MAT) and mean temperature of the coldest month (MTCO) from North America and Europe (Marsicek et al., 2018). (g) Time series of LIS deglaciation (Dyke, 2004). Gray shading indicates the Holocene temperature minimum at Lake E5 (d,e), which aligns with minima in DJFMAM insolation and GHG forcing (a-c). For the pollen synthesis, the Gray shading expands (f) to include the entire early Holocene, which was cool at mid-latitudes in North America and Eurasia in response to LIS retreat (g).

569

570 Given that orbital forcing during the summer and fall (JJASON) represents a larger  
 571 opposing forcing ( $15 \text{ w m}^{-2}$ ) than the combination of winter-spring (DJFMAM) insolation  
 572 and GHG forcing ( $4 \text{ w m}^{-2}$ ) over the last 7 ka, it is crucial to assess whether the mean  
 573 annual temperature (MAT) trend could have still been dominated by warming. Our  
 574 reconstruction suggests that it was, with Holocene winter-spring warming at Lake E5 (1.4

575 – 2.2 °C) featuring a greater amplitude than the opposing summer cooling (~ 0.5 – 1 °C)  
576 seen in a synthesis of terrestrial records from Alaska (Kaufman et al., 2016) and in a  
577 recent summer temperature reconstruction from the Yukon based on precipitation  
578 isotopes in syngenetic permafrost (Porter et al., 2019). GCM output generally support this  
579 conclusion as PMIP3 simulations suggest MATs at 6 ka did not exceed PI temperatures  
580 (Fig. 2). Indeed, new analysis of 6 ka climate simulations from the next phase of the  
581 Proxy Model Intercomparison Project (PMIP4), which improves upon PMIP3 by  
582 including realistic 6 ka GHG concentrations, shows more pronounced cooling at 6 ka vs.  
583 the PI for most parts of the world, including Alaska (Brierley et al., in review, 2020).  
584 Transient model simulations are more equivocal on whether mean annual temperature  
585 warmed or cooled in Alaska through the Holocene; two models (CCSM3 and  
586 LOVECLIM) indicate slight cooling in MAT while one model (FAMOUS) shows strong  
587 warming in MAT.

588

#### 589 *4.4. Regional Holocene Climate and Millennial-Scale Changes*

590

591 Terrestrial temperature records from Alaska and Yukon (Eastern Beringia) have primarily  
592 been interpreted to represent summer temperature changes. Quantitative midge-based  
593 summer temperature reconstructions suggest significant spatiotemporal temperature  
594 variability in the region, with some records showing early Holocene summer warmth  
595 (e.g. Kurek et al., 2009), while others suggest stable Holocene temperatures (Irvine et al.,  
596 2012). South-central Alaska differs further with midge reconstructions indicating non-  
597 linear responses to orbital forcing and a mid-Holocene thermal maximum (e.g. Clegg et

598 al., 2011). Pollen records have been used to reconstruct summer, winter and mean annual  
599 temperatures quantitatively through the Modern Analog Technique (Viau et al. 2008).  
600 However, these reconstructions may be compromised by non-analog pollen assemblages  
601 and broad ranges for key species in the transfer functions (Birks et al., 2011). Indeed, the  
602 quantitative pollen reconstructions are often at odds with qualitative pollen interpretations  
603 from the region (Viau et al., 2008). Taken at face-value, pollen reconstructions of  
604 summer temperature also suggest a mid-Holocene thermal maximum. Furthermore when  
605 pollen, midge and other geochemical records are combined into an Eastern Beringia  
606 composite, they suggest very little temperature change over the Holocene (<1 °C) due to  
607 the averaging out of spatiotemporal variations, but generally indicate a mid-Holocene  
608 thermal maximum roughly aligned with summer insolation forcing (Fig. 6b; Kaufman et  
609 al., 2016). Although this composite includes a limited number of marine records and  
610 records representing the cold seasons, it is dominated by records interpreted to reflect  
611 summer temperature over land.

612

613 In contrast to the summer- and terrestrial-dominated composite (Kaufman et al., 2016),  
614 marine records from the North Pacific and Arctic Ocean show more correspondence with  
615 winter-spring temperature changes at Lake E5. The 8 – 6 ka cal BP temperature  
616 minimum and subsequent warming trend at Lake E5 is captured in regional sea surface  
617 temperature (SST) records from the Chukchi Sea, Bering Sea and Gulf of Alaska (Fig. 6;  
618 McKay et al., 2008; Harada et al., 2014; Praetorius and Mix et al., 2014; locations shown  
619 in Fig. 1). Notably, these records were interpreted to reflect either mean annual or  
620 summer SST, but were likely sensitive to winter climate dynamics governing sea level

621 pressure and surface ocean and atmospheric circulation in the North Pacific (Trenberth  
622 and Hurrell, 1994). Additionally, sea ice reconstructions from the Beaufort and Chukchi  
623 Seas broadly indicate periods of reduced sea ice after 6 ka cal BP (Fig. 7; McKay et al.,  
624 2008; de Vernal et al., 2013; locations shown in Fig. 1). Ice in the Bering Sea forms  
625 during the winter months and is sensitive to winter-spring climate dynamics affecting ice  
626 formation and advection (Zhang et al., 2010). Bering Sea ice generally decreased after  
627 7.5 ka cal BP (Fig. 6; Katsuki et al., 2009, Harada et al., 2014), consistent with post-  
628 EMHT winter-spring warming. While sea ice concentrations likely responded to the same  
629 GHG forcing and winter-spring orbital forcing trends as our proxy record, they also  
630 impact terrestrial winter temperature and lake ice dynamics in northern Alaska (Alexeev  
631 et al., 2016) and therefore potentially amplified spring lake temperature changes. Overall,  
632 the agreement between these marine sites and the Lake E5 record demonstrates a  
633 coherent regional pattern of Holocene winter-spring temperature evolution driven by  
634 radiative forcing and potentially amplified by Northern Pacific atmosphere-ocean  
635 dynamics and sea ice feedbacks.

636

637 Although the sea ice records in the Chukchi and Bering Seas indicate reduced ice cover  
638 in the mid- to late Holocene, reconstructions from other regions within the Arctic Ocean  
639 and Nordic Seas demonstrate opposite features and trends (de Vernal et al., 2013). For  
640 example, ice cover expanded during the early Holocene in the Laptev Sea and maintained  
641 high levels through the middle and late Holocene (Fahl and Stein, 2012). Multiproxy  
642 records from the northern margin of Iceland indicate that sea ice export from the Arctic  
643 Ocean through the Fram Strait steadily increased through the mid-Holocene in step with

644 neoglaciation (Moros et al., 2006; Cabedo-Sanz et al., 2016). Together, the available sea  
645 ice records from the Arctic Ocean and adjacent seas suggest sea ice dynamics had unique  
646 regional patterns during the Holocene, likely in response to shifts in coupled atmosphere-  
647 ocean circulation patterns and relative changes in Fram Strait and Bering Strait  
648 throughflow (Darby et al., 2012; de Vernal et al., 2013). Therefore, Bering and Chukchi  
649 sea ice impacts on winter-spring temperature trends at Lake E5 were most likely regional  
650 in nature and may have been mitigated to some extent by differing pan-arctic sea ice  
651 trends during the Holocene.

652

653 In addition to the long-term Holocene trends, multi-centennial to millennial variability  
654 was a prominent feature of the Lake E5 record. Winter-spring temperatures show  
655 prominent local maxima centered on 5.2 and 1.4 ka cal BP (Fig. 6), with smaller events  
656 visible at 11, 9.5, 8.3 and 3.2 ka cal BP. Sea ice extent and sea ice drift reconstructions  
657 suggest that millennial-scale variability was a feature of Holocene climate in the  
658 Beaufort, and Chukchi Seas (Darby et al., 2012; de Vernal et al., 2013). Climate  
659 variability associated with changes in the strength and position of the Aleutian Low (AL)  
660 is broadly present in moisture sensitive records from southern Alaska (Anderson et al.,  
661 2005; Fisher et al., 2008; Kaufman et al., 2016) and has been shown to influence winter  
662 climate into interior Alaska (Clegg et al., 2010). While the direct impacts of the AL on  
663 Alaskan terrestrial climate are spatially complex (Anderson et al., 2015; Kaufman et al.,  
664 2016) there are several lines of evidence that the AL drove millennial-scale climate  
665 changes in Alaska (Kaufman et al., 2016). We suggest that millennial-scale winter-spring  
666 temperature oscillations in our reconstruction from Lake E5 were driven by a

667 combination of ocean-atmosphere dynamics associated with the Aleutian Low, and  
668 Arctic Ocean circulation changes controlling sea ice dynamics. Solar activity has been  
669 linked to higher frequency variability in the region (Hu et al., 2003) and indeed the  
670 general trend of increasing total solar irradiance from 8 to 4 ka cal BP (Steinhilber et al.,  
671 2012) is in agreement with winter-spring warming at Lake E5. However, higher  
672 frequency oscillations in total solar irradiance generally did not correlate with those in the  
673 Lake E5 record.

674

675 The most pronounced of the submillennial-scale changes observed during the Holocene  
676 at Lake E5 was a rapid warming of  $1.6 \pm 0.6$  °C around 5.8 ka cal BP (Table S2) that  
677 culminated in the temperature maxima at 5.2 ka cal BP. The event was recorded  
678 regionally in records of Chukchi Sea ice extent, Bering Strait through-flow and Gulf of  
679 Alaska SST (Fig. 6; McKay et al., 2008; Ortiz et al., 2009; Praetorius et al., 2015; Polyak  
680 et al., 2016). It is also a prominent feature of North American and European climate and  
681 aligns with mid-Holocene global change (Marsicek et al., 2019). Thus, millennial-scale  
682 variability in cold season temperatures at Lake E5 likely had both regional and global  
683 origins.

684

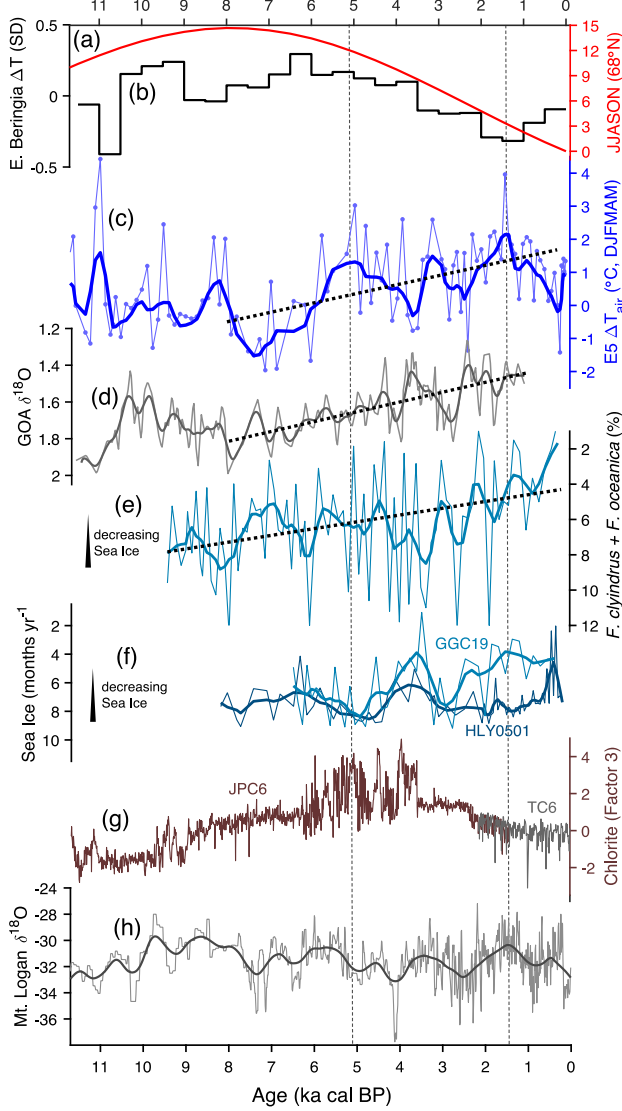


**Fig. 6. Holocene climate in Eastern Beringia.** (a) Mean insolation ( $\text{W m}^{-2}$ ,  $68^{\circ}\text{N}$ ) for the summer and fall (JJASON). (b) Composite of normalized summer and/or mean annual temperature reconstructions from Eastern Beringia (Kaufman et al., 2016). (c) Alkenone-inferred DJFMAM air temperature at Lake E5 shown as anomalies (vs. PI) and with 8 ka – PI trend. (d) Gulf of Alaska  $\delta^{18}\text{O}$  records from planktonic foraminifera interpreted as an indicator of mean annual SST (Praetorius and Mix, 2014). The record is shown with LOWESS smoothing and the post-EMHT trend. (e) Relative abundance of sea ice diatoms in core MR06-04-GC33 from the Bering Sea show with whole-record trend (Katsuki et al., 2009; Harada et al., 2014). (f) Dinocyst-based reconstructions of annual sea ice duration from Chuckchi Sea cores (McKay et al., 2008; de Vernal et al., 2013). (g) Proxy for Bering Strait throughflow based on chlorite transport to the Chukchi Sea from the North Pacific (Ortiz et al., 2009). (h) Mt. Logan ice core  $\delta^{18}\text{O}$  (Fisher et al., 2008). Vertical dotted lines highlight two millennial-scale winter-spring warm periods at Lake E5, which align with strengthened Bering strait throughflow and reduced Chukchi sea ice and Aleutian Low shifts, respectively.

685

686

687 **5. Conclusions**

688

689 This study provides the first quantitative alkenone-based reconstruction of Late Glacial  
690 and Holocene spring lake temperature change from Arctic Eastern Beringia. Our 16,000-  
691 year reconstruction from Lake E5 documents a series of rapid deglacial warming events  
692 that align with glacial retreat and paleo-ecological change in the region. Abrupt deglacial  
693 warming gave way to mild temperatures in the early Holocene and a long-term winter-  
694 spring warming trend. This trend occurred throughout the entire Holocene, but  
695 accelerated after 8 ka cal BP, corroborating surface temperature trends inferred from  
696 GCMs.

697

698 Our reconstruction supports the hypothesis that a warm season bias exists in regional and  
699 global proxy syntheses. Despite larger seasonal forcing from northern hemisphere  
700 summer insolation, winter-spring temperatures warmed considerably during the  
701 Holocene, balancing or exceeding summer cooling seen in a regional proxy synthesis  
702 from Eastern Beringia (Kaufman et al., 2016). Cold season temperature changes in our  
703 record, including early Holocene mild cooling followed by progressive warming since ~  
704 8 ka cal BP, mimic the pattern of change in GHG radiative forcing and cold season  
705 insolation, highlighting these factors, rather than ice sheet retreat, as the dominant climate  
706 drivers.

707 **Acknowledgements**

708 This work was funded by NSF grants PLR-1503846 to Y. Huang and J. Russell, PLR-  
709 1504069 to C. Morrill, and DEB-1637459 to E. Rastetter. Funding was also provided by  
710 a National Geographic Society Exploration Grant 9397-13 to Y. Huang, and a National  
711 Ocean Sciences Accelerator Mass Spectroscopy Internship to W. Longo. The project was  
712 greatly aided by logistical support from Toolik Field Station and limnological monitoring  
713 from the Arctic Long Term Ecological Research program (DEB-1637459). We thank X.  
714 Wang, P. Holland-Stergar and R. Tarozo for laboratory assistance. We acknowledge the  
715 World Climate Research Programme's Working Group on Coupled Modeling and the  
716 Paleoclimate Modelling Intercomparison Project for CMIP/PMIP model output. We  
717 thank two anonymous reviewers for feedback that significantly improved the manuscript.

718

719 **Competing Financial Interests**

720 The authors declare no competing financial interests.

721

722 **Data Availability**

723 Data presented in this manuscript are archived and publicly available at the National  
724 Science Foundation Arctic Data Center (doi:10.18739/A2CN6XZ7H).

725 **References**

726

727 Abbott, M.B., Edwards, M.E., Finney, B.P., 2010. A 40,000-yr record of environmental  
728 change from Burial Lake in Northwest Alaska. *Quat. Res.* 74, 156–165.

729 Alexeev, V.A., Arp, C.D., Jones, B.M., Cai, L., 2016. Arctic sea ice decline contributes  
730 to thinning lake ice trend in northern Alaska. *Environ. Res. Lett.* 11, 074022.

731 Anderson, L., Abbott, M.B., Finney, B.P., Burns, S.J., 2005. Regional atmospheric  
732 circulation change in the North Pacific during the Holocene inferred from lacustrine  
733 carbonate oxygen isotopes, Yukon Territory, Canada. *Quat. Res.* 64, 21–35.

734 Anderson, L., Berkelhammer, M., Barron, J.A., Steinman, B.A., Finney, B.P., Abbott,  
735 M.B., 2016. Lake oxygen isotopes as recorders of North American Rocky Mountain  
736 hydroclimate: Holocene patterns and variability at multi-decadal to millennial time  
737 scales. *Glob. Planet. Change* 137, 131–148.

738 Anderson, P.M., Brubaker, L.B., 1994. Vegetation history of northcentral Alaska: A  
739 mapped summary of late-quaternary pollen data. *Quat. Sci. Rev.* 13, 71–92.

740 ARC LTER database, 2016. Available from <<http://ecosystems.mbl.edu/ARC/datacatalog.html>>.

741 Arp, C.D., Jones, B.M., Grosse, G., 2013. Recent lake ice-out phenology within and  
742 among lake districts of Alaska, U.S.A. *Limnol. Oceanogr.* 58, 2013–2028.

743 Assel, R.A., Robertson, D.M., 1995. Changes in winter air temperatures near Lake  
744 Michigan, 1851–1993, as determined from regional lake-ice records. *Limonology*  
745 *Oceanogr.* 40, 165–176.

746 Baker, J.L., Lachniet, M.S., Chervyatsova, O., Asmerom, Y., Polyak, V.J., 2017.  
747 Holocene warming in western continental Eurasia driven by glacial retreat and  
748 greenhouse forcing. *Nat. Geosci.* 10.

749 Bartlein, P.J., Harrison, S.P., Brewer, S., Connor, S., Davis, B.A.S., Gajewski, K., Guiot,  
750 J., Harrison-Prentice, T.I., Henderson, A., Peyron, O., Prentice, I.C., Scholze, M.,  
751 Seppä, H., Shuman, B., Sugita, S., Thompson, R.S., Viau, A.E., Williams, J., Wu,  
752 H., 2011. Pollen-based continental climate reconstructions at 6 and 21 ka: A global  
753 synthesis. *Clim. Dyn.* 37, 775–802.

754 Birks, H.J.B., Heiri, O., Seppä, H., Bjune, A.E., 2011. Strengths and weaknesses of  
755 quantitative climate reconstructions based on late-Quaternary biological proxies.  
756 *Open Ecol. J.* 3, 68–110.

757 Braconnot, P., Harrison, S.P., Kageyama, M., Bartlein, P.J., Masson-Delmotte, V., Abe-  
758 Ouchi, A., Otto-Bliesner, B., Zhao, Y., 2012. Evaluation of climate models using  
759 palaeoclimatic data. *Nat. Clim. Chang.* 2, 417–424.

760 Bradley, R.S., England, J.H., 2008. The Younger Dryas and the Sea of Ancient Ice. *Quat.*  
761 *Res.* 70, 1–10.

762 Brassell, S.C., Eglinton, G., Marlowe, I.T., Pflaumann, U., Sarnthein, M., 1986.  
763 Molecular stratigraphy: a new tool for climatic assessment. *Nature* 320, 129–133.

764 Brierley et al. (in review, 2020) Large-scale features and evaluation of the PMIP4-  
765 CMIP6 midHolocene simulations. *Clim. Past Discuss.*, 10.5194/cp-2019-168

766 Cabedo-Sanz, P., Belt, S.T., Jennings, A.E., Andrews, J.T. and Geirsdóttir, Á., 2016.  
767 Variability in drift ice export from the Arctic Ocean to the North Icelandic Shelf  
768 over the last 8000 years: a multi-proxy evaluation. *Quat. Sci. Rev.* 146, 99–115.

769 Caissie, B.E., Brigham-Grette, J., Lawrence, K.T., Herbert, T.D., Cook, M.S., 2010. Last

770

771       Glacial Maximum to Holocene sea surface conditions at Umnak Plateau, Bering  
772       Sea, as inferred from diatom, alkenone, and stable isotope records.  
773       Paleoceanography 25, PA1206.

774       Clark, P.U., Alley, R.B., Pollard, D., 1999. Northern Hemisphere Ice-Sheet Influences on  
775       Global Climate Change. *Science* (80-). 286, 1104–1112.

776       Clegg, B.F., Hu, F.S., 2010. An oxygen-isotope record of Holocene climate change in the  
777       south-central Brooks Range, Alaska. *Quat. Sci. Rev.* 29, 928–939.

778       Clegg, B.F., Kelly, R., Clarke, G.H., Walker, I.R., Sheng, F., 2011. Nonlinear response of  
779       summer temperature to Holocene insolation forcing in Alaska *Proc. Natl. Acad. Sci.*  
780       U. S. A.

781       Conte, M.H., Sicre, M.-A., Röhleemann, C., Weber, J.C., Schulte, S., Schulz-Bull, D.,  
782       Blanz, T., 2006. Global temperature calibration of the alkenone unsaturation index  
783       (UK'37) in surface waters and comparison with surface sediments. *Geochemistry,*  
784       *Geophys. Geosystems* 7, 10.1029/2005GC001054.

785       D'Andrea, W.J., Huang, Y., Fritz, S.C., Anderson, N.J., 2011. Abrupt Holocene climate  
786       change as an important factor for human migration in West Greenland. *Proc. Natl.*  
787       *Acad. Sci. U. S. A.* 108, 9765–9.

788       D'Andrea, W.J., Lage, M., Martiny, J.B.H., Laatsch, A.D., Amaral-Zettler, L. a., Sogin,  
789       M.L., Huang, Y., 2006. Alkenone producers inferred from well-preserved 18S  
790       rDNA in Greenland lake sediments. *J. Geophys. Res.* 111, G03013.

791       D'Andrea, W.J., Theroux, S., Bradley, R.S., Huang, X., 2016. Does phylogeny control  
792       UK37-temperature sensitivity? Implications for lacustrine alkenone  
793       paleothermometry. *Geochim. Cosmochim. Acta* 175, 168–180.

794       Darby, D.A., Ortiz, J.D., Grosch, C.E., Lund, S.P., 2012. 1,500-year cycle in the Arctic  
795       Oscillation identified in Holocene Arctic sea-ice drift. *Nat. Geosci.* 5, 897–900.

796       de Vernal, A., Hillaire-marcel, C., Rochon, A., Fréchette, B., Henry, M., Solignac, S.,  
797       Bonnet, S., 2013. Dinocyst-based reconstructions of sea ice cover concentration  
798       during the Holocene in the Arctic Ocean, the northern North Atlantic Ocean and its  
799       adjacent seas. *Quat. Sci. Rev.* 79, 111–121.

800       Dee, S.G., Russell, J.M., Morrill, C., Chen, Z., Neary, A., 2018. PRYSM v2 . 0 : A Proxy  
801       System Model for Lacustrine Archives. *Paleoceanogr. Paleoclimatology*.

802       Denton, G.H., Alley, R.B., Comer, G.C., Broecker, W.S., 2005. The role of seasonality in  
803       abrupt climate change. *Quat. Sci. Rev.* 24, 1159–1182.

804       Déry, S.J., Stieglitz, M., Rennermalm, Å.K., Wood, E.F., 2005. The Water Budget of the  
805       Kuparuk River Basin, Alaska. *J. Hydrometeorol.* 6, 633–655.

806       Dyke, A.S., 2004. An outline of North American deglaciation with emphasis on central  
807       and northern Canada, in: Ehlers, J., Gibbard, P. (Eds.), *Developments in Quaternary*  
808       *Sciences*. Elsevier B.V., pp. 373–424.

809       Eisner, W.R., Colinvaux, P.A., 1992. Late Quaternary Pollen Records from Oil Lake and  
810       Feniak Alaska, U.S.A. *Arct. Alp. Res.* 24, 56–63.

811       Environmental Data Center Team. 2016. Meteorological monitoring program at Toolik,  
812       Alaska. Toolik Field Station, Institute of Arctic Biology, University of Alaska  
813       Fairbanks, Fairbanks, AK 99775.  
814       [http://toolik.alaska.edu/edc/abiotic\\_monitoring/data\\_query.php](http://toolik.alaska.edu/edc/abiotic_monitoring/data_query.php)

815       Fahl, K. and Stein, R., 2012. Modern seasonal variability and deglacial/Holocene change

816 of central Arctic Ocean sea-ice cover: New insights from biomarker proxy records.  
817 *Earth Planet. Sci. Lett.* 351, pp.123-133.

818 Fisher, D., Osterberg, E., Dyke, A., Dahl-jensen, D., Demuth, M., Zdanowicz, C.,  
819 Bourgeois, J., Roy, M., Mayewski, P., Wake, C., Kreutz, K., Zheng, J., Yalcin, K.,  
820 Goto-azuma, K., Rupper, S., 2008. The Mt Logan Holocene – late Wisconsinan  
821 isotope record : tropical Pacific – Yukon connections 5, 667–677.

822 Foley, J.A., Kutzbach, J.E., Coe, M.T., Levis, S., 1994. Feedbacks between climate and  
823 boreal forests during the Holocene epoch. *Nature* 371, 52–54.

824 Gaglioti, B. V, Mann, D.H., Wooller, M.J., Jones, B.M., Wiles, G.C., Groves, P., Kunz,  
825 M.L., Baughman, C.A., Reanier, R.E., 2017. Younger-Dryas cooling and sea-ice  
826 feedbacks were prominent features of the Pleistocene-Holocene transition in Arctic  
827 Alaska. *Quat. Sci. Rev.* 169, 330–343.

828 Hamilton, T.D., 1982. A late Pleistocene glacial chronology for the southern Brooks  
829 Range: Stratigraphic record and regional significance. *Geol. Soc. Am. Bull.* 93,  
830 700–716.

831 Harada, N., Katsuki, K., Nakagawa, M., Matsumoto, A., Seki, O., Addison, J. a., Finney,  
832 B.P., Sato, M., 2014. Holocene sea surface temperature and sea ice extent in the  
833 Okhotsk and Bering Seas. *Prog. Oceanogr.* 126, 242–253.

834 Hu, F.S., Kaufman, D., Yoneji, S., Nelson, D., Shemesh, A., Huang, Y., Tian, J., Bond,  
835 G., Clegg, B. and Brown, T., 2003. Cyclic variation and solar forcing of Holocene  
836 climate in the Alaskan subarctic. *Science* 301(5641), 1890-1893.

837 Huryn, A. and Hobbie, J., 2012. Land of extremes: a natural history of the Arctic North  
838 Slope of Alaska. University of Alaska Press.

839 Hostetler, S., Bartlein, P., 1990. Simulation of Lake Evaporation with Application to  
840 Modeling Lake Level Variations, Oregon. *Water Resour. Res.* 26, 2603–2612.

841 Irvine, F., Cwynar, L.C., Vermaire, J.C., Rees, A.B.H., 2012. Midge-inferred temperature  
842 reconstructions and vegetation change over the last ~15,000 years from Trout Lake,  
843 northern Yukon Territory, eastern Beringia. *J. Paleolimnol.* 48, 133–146.

844 Joos, F., Spahni, R., 2008. Rates of change in natural and anthropogenic radiative forcing  
845 over the past 20,000 years. *Proc. Natl. Acad. Sci.* 105, 1425–1430.

846 Katsuki, K., Khim, B.-K., Itaki, T., Harada, N., Sakai, H., Ikeda, T., Takahashi, K.,  
847 Okazaki, Y., Asahi, H., 2009. Land-sea linkage of Holocene paleoclimate on the  
848 Southern Bering Continental Shelf. *The Holocene* 19, 747–756.

849 Kaufman, D., 2004. Holocene thermal maximum in the western Arctic (0–180°W). *Quat.*  
850 *Sci. Rev.* 23, 529–560.

851 Kaufman, D.S., Axford, Y.L., Henderson, A.C.G., McKay, N.P., Oswald, W.W.,  
852 Saenger, C., Anderson, R.S., Bailey, H.L., Clegg, B., Gajewski, K., Hu, F.S., Jones,  
853 M.C., Massa, C., Routson, C.C., Werner, A., Wooller, M.J., Yu, Z., 2016. Holocene  
854 climate changes in eastern Beringia (NW North America) – A systematic review of  
855 multi-proxy evidence. *Quat. Sci. Rev.* 147, 312–339.

856 Kaufman, D.S., Schneider, D.P., McKay, N.P., Ammann, C.M., Bradley, R.S., Briffa,  
857 K.R., Miller, G.H., Otto-Bliesner, B.L., Overpeck, J.T., Vinther, B.M., 2009. Recent  
858 warming reverses long-term arctic cooling. *Science* 325, 1236–9.

859 Kokorowski, H.D., Anderson, P.M., Mock, C.J., Lozhkin, A. V., 2008. A re-evaluation  
860 and spatial analysis of evidence for a Younger Dryas climatic reversal in Beringia.  
861 *Quat. Sci. Rev.* 27, 1710–1722.

862 Kurek, J., Cwynar, L.C., Ager, T.A., Abbott, M.B., Edwards, M.E., 2009. Late  
863 Quaternary paleoclimate of western Alaska inferred from fossil chironomids and its  
864 relation to vegetation histories. *Quat. Sci. Rev.* 28, 799–811.

865 Laskar, J., Robutel, P., Joutel, F., Gastineau, M., Correia, a. C.M., Levrard, B., 2004. A  
866 long-term numerical solution for the insolation quantities of the Earth. *Astron. Astrophys.* 428, 261–285.

867 Liu, Z., He, F., Brady, E.C., Tomas, R., Clark, P.U., Carlson, A.E., Curry, W., Brook, E.,  
868 Erickson, D., Jacob, R., Kutzbach, J., Cheng, J., 2009. Transient Simulation of Last  
869 Deglaciation with a New Mechanism for Bølling-Allerød Warming. *Science* (80-. ).  
870 413, 310–315.

871 Liu, Z., Zhu, J., Rosenthal, Y., Zhang, X., Otto-Bliesner, B.L., Timmermann, A., Smith,  
872 R.S., Lohmann, G., Zheng, W., Timm, O.E., 2014. The Holocene temperature  
873 conundrum. *Proc. Natl. Acad. Sci.* 111, E3501–E3505.

874 Livingstone, D.M., 1997. Break-up dates of Alpine lakes as proxy data for local and  
875 regional mean surface air temperatures. *Clim. Change* 37, 407–439.

876 Longo, W.M., Dillon, J.T., Tarozo, R., Salacup, J.M., Huang, Y., 2013. Unprecedented  
877 separation of long chain alkenones from gas chromatography with a  
878 poly(trifluoropropylmethylsiloxane) stationary phase. *Org. Geochem.* 65, 94–102.

879 Longo, W.M., Huang, Y., Yao, Y., Zhao, J., Giblin, A.E., Wang, X., Zech, R., Haberzettl,  
880 T., Jardillier, L., Toney, J., Liu, Z., Krivonogov, S., Kolpakova, M., Chu, G.,  
881 D'Andrea, W.J., Harada, N., Nagashima, K., Sato, M., Yonenobu, H., Yamada, K.,  
882 Gotanda, K., Shinozuka, Y., 2018. Widespread occurrence of distinct alkenones  
883 from Group I haptophytes in freshwater lakes: Implications for paleotemperature  
884 and paleoenvironmental reconstructions. *Earth Planet. Sci. Lett.* 492, 239–250.

885 Longo, W.M., Theroux, S., Giblin, A.E., Zheng, Y., James, T., Huang, Y., Longo, W.M.,  
886 Theroux, S., Giblin, A.E., Zheng, Y., Dillon, J.T., Huang, Y., 2016. Temperature  
887 calibration and phylogenetically distinct distributions for freshwater alkenones:  
888 Evidence from northern Alaskan lakes. *Geochim. Cosmochim. Acta* 180, 177–196.

889 Magnuson, J.J., Robertson, D.M., Benson, B.B., Wynne, R.H., Livingstone, D.M., Arai,  
890 T., Assel, R.A., Barry, R.G., Card, V., Kuusisto, E., Granin, N.G., Prowse, T.,  
891 Stewart, K.M., Vuglinski, V.S., 2000. Historical Trends in Lake and River Ice Cover  
892 in the Northern Hemisphere. *Science* (80-. ). 289, 1743–1746.

893 Manley, W.F., 2002. Postglacial flooding of the bering land Bridge: a geospatial  
894 animation v1. INSTAAR. WWW Document. [http://instaar.colorado.edu/QGISL/bering\\_land\\_bridge1](http://instaar.colorado.edu/QGISL/bering_land_bridge1).

895 Mann, D.H., Groves, P., Reanier, R.E., Kunz, M.L., 2010. Floodplains, permafrost,  
896 cottonwood trees, and peat: What happened the last time climate warmed suddenly  
897 in arctic Alaska? *Quat. Sci. Rev.* 29, 3812–3830.

898 Mann, D.H., Peteet, D.M., Reanier, R.E., Kunz, M.L., 2002. Responses of an arctic  
899 landscape to Lateglacial and early Holocene climatic changes: the importance of  
900 moisture. *Quat. Sci. Rev.* 21, 997–1021.

901 Marcott, S.A., Shakun, J.D., Clark, P.U., Mix, A.C., 2013. A Reconstruction of Regional  
902 and Global Temperature for the Past 11,300 Years. *Science* 339, 1198–1201.

903 Marlowe, I.T., Green, J.C., Neal, A.C., Brassell, S.C., Eglinton, G., Course, P.A., 1984.  
904 Long chain (n-C<sub>37</sub> – C<sub>39</sub>) alkenones in the Prymnesiophyceae. Distribution of  
905 alkenones and other lipids and their taxonomic significance. *Br. Phycol. J.* 19, 203–

906

907

908 216.

909 Marsicek, J., Shuman, B.N., Bartlein, P.J., Shafer, S.L., Brewer, S., 2018. Reconciling  
910 divergent trends and millennial variations in Holocene temperatures. *Nature* 554,  
911 92–96.

912 Mayewski, P.A., Rohling, E.E., Stager, J.C., Karl??n, W., Maasch, K.A., Meeker, L.D.,  
913 Meyerson, E.A., Gasse, F., van Kreveld, S., Holmgren, K., Lee-Thorp, J., Rosqvist,  
914 G., Rack, F., Staubwasser, M., Schneider, R.R., Steig, E.J., 2004. Holocene climate  
915 variability. *Quat. Res.* 62, 243–255.

916 McKay, J.L., de Vernal, A., Hillaire-Marcel, C., Not, C., Polyak, L., Darby, D., 2008.  
917 Holocene fluctuations in Arctic sea-ice cover: dinocyst-based reconstructions for the  
918 eastern Chukchi Sea. *Can. J. Earth Sci.* 45, 1377–1397.

919 Meyer, H., Opel, T., Laepple, T., Dereviagin, A.Y., Hoffmann, K., Werner, M., 2015.  
920 Long-term winter warming trend in the Siberian Arctic during the mid- to late  
921 Holocene. *Nat. Geosci.* 8, 122–125.

922 Meyer, H., Schirrmeyer, L., Yoshikawa, K., Opel, T., Wetterich, S., Hubberten, H.W.,  
923 Brown, J., 2010. Permafrost evidence for severe winter cooling during the Younger  
924 Dryas in northern Alaska. *Geophys. Res. Lett.* 37, 1–5.

925 Monnin, E., Indermühle, a, Dällenbach, a, Flückiger, J., Stauffer, B., Stocker, T.F.,  
926 Raynaud, D., Barnola, J.M., 2001. Atmospheric CO<sub>2</sub> concentrations over the last  
927 glacial termination. *Science* 291, 112–114.

928 Moros, M., Andrews, J.T., Eberl, D.D. and Jansen, E., 2006. Holocene history of drift ice  
929 in the northern North Atlantic: Evidence for different spatial and temporal modes.  
930 *Paleoceanogr.* 21(2).

931 Opel, T., Meyer, H., Wetterich, S., Laepple, T., Dereviagin, A. and Murton, J., 2018. Ice  
932 wedges as archives of winter paleoclimate: A review. *Permafrost and Periglacial  
933 Processes*, 29(3), pp.199-209.

934 Ortiz, J.D., Polyak, L., Grebmeier, J.M., Darby, D., Eberl, D.D., Naidu, S., Nof, D., 2009.  
935 Provenance of Holocene sediment on the Chukchi-Alaskan margin based on  
936 combined diffuse spectral reflectance and quantitative X-Ray Diffraction analysis.  
937 *Glob. Planet. Change* 68, 73–84.

938 Palecki, M.A., Barry, R.G., 1986. Freeze-up and Break-up of Lakes as an Index of  
939 Temperature Changes during the Transition Seasons: A Case Study for Finland. *J.  
940 Clim. Appl. Meteorol.* 25, 893–902.

941 Pendleton, S.L., Ceperley, E.G., Briner, J.P., Kaufman, D.S., Zimmerman, S., 2015.  
942 Rapid and early deglaciation in the central Brooks Range, Arctic Alaska. *Geology*  
943 43, 419–422.

944 Polyak, L., Belt, S.T., Cabedo-Sanz, P., Yamamoto, M., Park, Y.-H., 2016. Holocene sea-  
945 ice conditions and circulation at the Chukchi-Alaskan margin, Arctic Ocean,  
946 inferred from biomarker proxies. *The Holocene* 26, 1810–1821.

947 Porter, T.J., Schoenemann, S.W., Davies, L.J., Steig, E.J., Bandara, S. and Froese, D.G.,  
948 2019. Recent summer warming in northwestern Canada exceeds the Holocene  
949 thermal maximum. *Nat. Commun.* 10(1), 1-10.

950 Praetorius, S.K., Mix, A.C., 2014. Synchronization of North Pacific and Greenland  
951 climates preceded abrupt deglacial warming. *Science* (80-). 345, 444–448.

952 Praetorius, S.K., Mix, A.C., Walczak, M.H., Wolhowe, M.D., Addison, J.A., Prahl, F.G.,  
953 2015. North Pacific deglacial hypoxic events linked to abrupt ocean warming.



996